Thermal and Electric Conductivities of Coulomb Crystals in the Inner Crust of a Neutron Star

D.A. Baiko and D.G. Yakovlev
Ioffe Physical Technical Institute, St.Petersburg
Received on November 17, 1995

Abstract

Thermal and electric conductivities of relativistic degenerate electrons are calculated for the case when electrons scatter by phonons in Coulomb crystals made of spherical finite–size nuclei at densities 10^{11} g/cm^3 $\lesssim \rho \lesssim 10^{14}$ g/cm^3, corresponding to the inner crust of a neutron star. In combination with the results of the previous article (for lower ρ), simple unified fits are obtained which describe the kinetic coefficients in the range 10^3 g/cm^3 $\lesssim \rho \lesssim 10^{14}$ g/cm^3, for matter with arbitrary nuclear composition. The results are valid for studying thermal evolution of neutron stars and evolution of their magnetic fields. The difference between the kinetic coefficients in the neutron star crust composed of ground state and accreted matters is analyzed. Thermal drift of the magnetic field in the neutron star crust is discussed.

1 INTRODUCTION

The thermal end electrical conductivities of degenerate electrons which suffer electron–phonon scattering in Coulomb crystals of atomic nuclei in dense matter of white dwarfs and neutron stars has been studied by a number of authors. In particular, Yakovlev and Urpin (1980) developed an approximate method of evaluation of the kinetic coefficients which takes into account the main features of phonon spectrum in the body-centered-cubic Coulomb crystals and the leading role of the Umklapp processes in electron–phonon scattering under astrophysical conditions. The same authors presented critical analysis of the preceding papers. Raikh and Yakovlev (1982) confirmed the validity of the approximate method by direct Monte Carlo calculations of the kinetic coefficients with allowance for the exact phonon spectrum and contributions from the normal and Umklapp scattering processes. Itoh et al. (1984, 1993) used the same approximate method but included the Debye – Waller factor. These authors fitted their results by very complicated expressions. Finally, Baiko and Yakovlev (1995) calculated the kinetic coefficients directly by the Monte Carlo method and by the approximate analytic method, including the Debye – Waller factor, in the density range 10^3 g/cm^3 $\lesssim \rho \lesssim 10^{11}$ g/cm^3, which corresponds to the cores of white dwarfs and outer crusts of neutron stars. Monte Carlo simulations confirmed the validity of the results of Itoh et al. (1984, 1993) obtained by the approximate method. The analytic approach allowed Baiko and Yakovlev (1995) to fit the kinetic coefficients by simple equations, valid for any nuclear composition, and to extend the results to the case of the face-centered-cubic Coulomb crystals, which could also exist in dense stellar matter but which had not been considered earlier.

The aim of the present article is to study the kinetic coefficients at higher densities 10^{11} g/cm^3 $\lesssim \rho \lesssim 10^{14}$ g/cm^3. This range corresponds to the inner crust of a neutron star where finite sizes of atomic nuclei are important. Combining the results of the present article and the analytic fits of Baiko and Yakovlev (1995) for lower densities, we will obtain simple fit expressions valid equally for the outer and inner crusts of neutron stars with any nuclear composition.

2 GENERAL RELATIONSHIPS

Consider cold matter in the density range 10^{11} g/cm^3 $\lesssim \rho \lesssim 10^{14}$ g/cm^3. At $\rho < \rho_{\rm d}$ ($\rho_{\rm d} \approx (4-6) \times 10^{11}$ g/cm^3 is the neutron drip density) matter consists of nuclei (Z, A) and strongly degenerate, ultrarelativistic and almost ideal electrons. We assume that, at fixed ρ and T, there are nuclei of single species. Highly energetic electrons induce β captures and, therefore, large neutron excess of atomic nuclei (e.g., Shapiro and Teukolsky, 1983). At higher densities, $\rho_{\rm d} < \rho \lesssim 10^{14}$ g/cm^3, matter contains also free neutrons in addition to the nuclei and electrons. With the grows of ρ, the fraction of the neutrons increases. At $\rho \gtrsim 10^{14}$ g/cm^3 the nuclei may become nonspherical and/or form clusters (Lorenz et al., 1993). The nuclear composition depends on pre-history of the neutron star

crust. For instance, the composition of ground state matter (Negele and Vautherin, 1973; Haensel and Pichon, 1994) differs noticeably from that of accreted matter (Haensel and Zdunik, 1990 a, b).

The properties of matter depend also on temperature T. At low T the nuclei (ions) form Coulomb crystal. One commonly studies body-centered-cubic crystals which are most tightly bound. However the difference of binding energies of the body-centered-cubic and face-centered-cubic crystals is very small, and one cannot exclude the presence of face-centered-cubic crystals in the neutron star crust (e.g., Baiko and Yakovlev, 1995). The classical body-centered-cubic crystal melts when the ion coupling parameter $\Gamma \equiv Z^2e^2/(ak_{\rm B}T)$ reaches the critical value $\Gamma = \Gamma_{\rm m} \approx 172$ (Nagara et al., 1987). In this case $a = [3/(4\pi n_{\rm i})]^{1/3}$ is the mean inter-ion distance, $n_{\rm i}$ is the number density of the nuclei, and $k_{\rm B}$ is the Boltzmann constant. Accordingly, the melting temperature is (Figures 1 and 2)

$$T_{\rm m} = \frac{Z^2e^2}{ak_{\rm B}\Gamma_{\rm m}} \approx 1.323 \times 10^5 Z^{5/3} \left(\frac{\rho_6}{\mu_{\rm e}}\right)^{1/3} \frac{172}{\Gamma_{\rm m}}\ {\rm K}, \qquad (1)$$

where $\mu_{\rm e}$ is the number of baryons per one electron, ρ_6 is density in units of 10^6 g/cm^3.

The thermal and electric conduction in crystalline matter ($T < T_{\rm m}$) is mainly provided by the electrons due to the electron–phonon scattering. Under astrophysical conditions, the normal and Umklapp scattering processes are allowed (e.g, Raikh and Yakovlev, 1982). The scattering regime is determined by the relationship between the temperature T and the ion plasma temperature (Figures 1 and 2)

$$T_{\rm p} = \frac{\hbar\omega_p}{k_{\rm B}} \approx 7.832 \times 10^6 \sqrt{\frac{Z\rho_6}{A\mu_e}}\ {\rm K}, \qquad (2)$$

where $\omega_{\rm p} = \sqrt{4\pi Z^2e^2n_{\rm i}/m_{\rm i}}$ is the ion plasma frequency and $m_{\rm i}$ is the ion mass. Note that the Debye temperature of the crystal is $T_{\rm D} = 0.45T_{\rm p}$ (Carr, 1961). If $T \gtrsim T_{\rm p}$, many thermal phonons are excited, and the electron scattering can be treated classically (as caused by thermal lattice vibrations). At $T \ll T_{\rm p}$ the number of thermal phonons is strongly reduced, and the scattering is essentially quantum (involves single phonons). In the both cases the Umklapp processes dominate the normal ones. However, at very low temperatures $T \ll T_{\rm U}$ (Figures 1 and 2), the Umklapp processes are frozen out, and the normal processes become more significant (e.g., Raikh and Yakovlev, 1982). Here, $T_{\rm U} \sim T_{\rm p}Z^{1/3}e^2/(\hbar v_{\rm F})$, $v_{\rm F} \approx c$ being the electron Fermi velocity. We shall restrict ourselves to the case of $T \gtrsim T_{\rm U}$, which is most important for applications. In this case, one can use the free electron approximation.

We express the thermal conductivity κ and electric conductivity σ through the effective electron collision frequencies ν_κ and ν_σ:

$$\kappa \ = \ \frac{\pi^2{k_{\rm B}}^2Tn_{\rm e}}{3m_*\nu_\kappa} \approx 4.04 \times 10^{15} x^2 \beta T_6 \left(\frac{10^{16-1}}{\nu_\kappa}\right) \ \frac{\rm ergs}{\rm cm\ s\ K},$$

$$\sigma = \frac{e^2 n_{\rm e}}{m_* \nu_\sigma} \approx 1.49 \times 10^{22} x^2 \beta \left(\frac{10^{16-1}}{\nu_\sigma}\right) \ \frac{1}{\rm s}. \quad (3)$$

In this case $x = p_{\rm F}/(m_{\rm e}c)$, $\beta = v_{\rm F}/c = x/\sqrt{1+x^2}$, $m_* = m_{\rm e}\sqrt{1+x^2}$, and $p_{\rm F}$ is the electron Fermi momentum.

The frequencies ν_κ and ν_σ are conveniently expressed (Yakovlev and Urpin, 1980) through the dimensionless functions F_σ and F_κ:

$$\nu_{\sigma,\kappa} = \frac{e^2}{\hbar v_{\rm F}} \frac{k_{\rm B}T}{\hbar} F_{\sigma,\kappa} \approx 0.955 \times 10^{15} \frac{T_6}{\beta} F_{\sigma,\kappa} \ \ {\rm s}^{-1}. \quad (4)$$

For calculating these functions, we will use the approximate formulae derived by Baiko and Yakovlev (1995). The general formalism is independent of lattice type. The cases of the body-centered-cubic and face-centered-cubic crystals differ through numerical factors determined by phonon spectrum. According to Baiko and Yakovlev (1995),

$$F_\sigma = G_0(t) K_0, \quad F_\kappa = F_\sigma + G_2(t)\left(3K_2 - \frac{1}{2}K_0\right), \quad (5)$$

$$\begin{aligned} K_0 &= \int_{q_{\rm min}}^{2k_{\rm F}} \frac{\hbar^2 q\,{\rm d}q}{p_{\rm F}^2} \frac{|f(q)|^2}{|\epsilon(q)|^2}\left(1 - \frac{\beta^2\hbar^2 q^2}{4p_{\rm F}^2}\right) {\rm e}^{-2W} \\ &= 2\int_{u_0}^{1} {\rm d}u \, \frac{|f(q)|^2}{|\epsilon(q)|^2}\left(1-\beta^2 u\right) {\rm e}^{-2W}, \\ K_2 &= \int_{q_{\rm min}}^{2k_{\rm F}} \frac{{\rm d}q}{q} \frac{|f(q)|^2}{|\epsilon(q)|^2}\left(1 - \frac{\beta^2\hbar^2 q^2}{4p_{\rm F}^2}\right) {\rm e}^{-2W} \\ &= \frac{1}{2}\int_{u_0}^{1} \frac{{\rm d}u}{u} \frac{|f(q)|^2}{|\epsilon(q)|^2}\left(1-\beta^2 u\right) {\rm e}^{-2W}. \end{aligned} \quad (6)$$

Here, $\hbar q$ is the momentum transferred by an electron due to emission or absorption of a phonon, $u = [\hbar q/(2p_{\rm F})]^2$, $t = T/T_{\rm p}$ is the dimensionless temperature, ${\rm e}^{-2W}$ is the Debye — Waller factor, $f(q)$ is the nuclear formfactor, $\epsilon(q)$ is the static longitudinal dielectric function of the degenerate electron gas (Jancovici, 1962). The lower limit of integration over q ($q = q_{\rm min}$) restricts the integration domain where the Umklapp processes are operative (e.g., Raikh and Yakovlev, 1982); this limit is set equal to the equivalent radius of the Brillouin zone $q_{\rm min} = (6\pi^2 n_{\rm i})^{1/3}$; $u_0 = [\hbar q_{\rm min}/(2p_{\rm F})]^2 = 1/(4Z)^{2/3}$.

The functions G_0 and G_2 in Equations (5) are determined by the phonon spectrum. They have been calculated and fitted by Yakovlev and Urpin (1980), Raikh and Yakovlev (1982), and also by Baiko and Yakovlev (1995):

$$\begin{aligned} G_0(t) &= \frac{u_{-2}t}{\sqrt{t^2+a_0}}, \\ G_2(t) &= \frac{t}{\pi^2(t^2+a_2)^{3/2}}. \end{aligned} \quad (7)$$

In this case u_{-2}, a_0 and a_2 are the constants determined by the lattice type and u_{-2} is a frequency moment of the phonon spectrum. For the body-centered-cubic crystal, we have $u_{-2}^{(\mathrm{bcc})} = 13.00$, $a_0^{(\mathrm{bcc})} = 0.0174$ and $a_2^{(\mathrm{bcc})} = 0.0118$. For the face-centered-cubic crystal, $u_{-2}^{(\mathrm{fcc})} = 28.80$, $a_0^{(\mathrm{fcc})} = 0.00505$ and $a_2^{(\mathrm{fcc})} = 0.00461$.

As shown by Baiko and Yakovlev (1995), the Debye – Waller parameter can be fitted (with the mean error of $\sim 1\%$) as

$$\begin{aligned} 2W(q) &= \alpha u, \\ \alpha &= \alpha_0 \left(\frac{1}{2} u_{-1} \mathrm{e}^{-9.100t} + t u_{-2}\right), \\ \alpha_0 &= \frac{4 m_\mathrm{e}^2 c^2}{k_\mathrm{B} T_\mathrm{p} m_\mathrm{i}} x^2 \approx 1.683 \sqrt{\frac{x}{AZ}}, \end{aligned} \tag{8}$$

where u_{-1} is another frequency moment of the phonon spectrum, $u_{-1}^{(\mathrm{bcc})} = 2.800$, $u_{-1}^{(\mathrm{fcc})} = 4.03$.

Since we consider the ultrarelativistic electron gas, it is sufficient to set $x \gg 1$, $\beta = 1$.

For the densities of interest, the sizes of atomic nuclei become comparable to the interion distance a (see above). Contrary to the case of $\rho \lesssim 10^{11}$ g/cm^3, considered by Baiko and Yakovlev (1995), the nuclear formfactor $f(q)$ becomes important in the integrals (6). We will not analyze the nonspherical nuclei which may appear at $\rho \gtrsim 10^{14}$ g/cm^3 (Lorenz et al., 1993), but restrict ourselves to a standard model of spherical nuclei with the uniform proton core of radius r_c:

$$\begin{aligned} f(q) &= \frac{3}{(qr_\mathrm{c})^3} \left[\sin(qr_\mathrm{c}) - qr_\mathrm{c} \cos(qr_\mathrm{c})\right], \\ qr_\mathrm{c} &= \sqrt{u}\, \frac{r_\mathrm{c}}{a} \left(18\pi Z\right)^{1/3}. \end{aligned} \tag{9}$$

3 NUMERICAL RESULTS AND THEIR APPROXIMATION

Calculation of the thermal and electric conductivities reduces to evaluating the integrals K_0 and K_2 from Equations (6). For the conditions of study, the functions K_0 and K_2 depend on three parameters: on the quantity α in the Debye — Waller factor (8), on the nuclear charge number Z and on the parameter $g = r_\mathrm{c}/a$ in the nuclear formfactor (9). We have calculated the integrals (6) at $Z = 20, 40, 60$, $\alpha = 0.04$, 0.12, 0.4, 1.2, 4, 12, and $g =$ 0, 0.1, 0.2, 0.3, 0.4. Analyzing the properties of matter at 10^{11} g/cm$^3 \lesssim \rho \lesssim 10^{14}$ g/cm^3, one can see (Section 4) that the adopted grid covers all possible parameter domain.

Let us fit the newly calculated values of K_σ and K_κ basing on the analytic expressions for F_σ and F_κ at $\rho \lesssim 10^{11}$ g/cm^3 obtained by Baiko and Yakovlev (1995). First of all, note that the electric screening is rather insignificant. As shown by Baiko and Yakovlev (1995), one can set $\epsilon(q)$=1 in the integrals (6) and include the weak screening effect by shifting

the integration limit u_0 to $u_1 = (4Z)^{-2/3} + u_e$, where $u_e = [\hbar k_{\rm TF}/(2p_{\rm F})]^2 = e^2/(\pi\hbar v_{\rm F}) \approx 1/(137\pi\beta)$ and $k_{\rm TF}$ is the inverse length of screening of a charge by the degenerate plasma electrons.

First consider the small–size nuclei ($g \ll 1$). Expanding the formfactor up to the terms $\propto g^2$, we obtain $|f(q)|^2 \approx 1 - 0.2(qr_{\rm c})^2$. Then the integrals (6) are taken:

$$K_0 = 2\Phi_1 - \frac{2}{5}\left(\frac{2p_{\rm F}r_{\rm c}}{\hbar}\right)^2 \Phi_2, \quad K_2 = \frac{1}{2}\Phi_0 - \frac{1}{10}\left(\frac{2p_{\rm F}r_{\rm c}}{\hbar}\right)^2 \Phi_1. \tag{10}$$

Here, we have introduced the functions

$$\Phi_k = S_{k-1} - \beta^2 S_k, \quad S_k = \int_{u_1}^{1} {\rm d}u\, u^k\, {\rm e}^{-\alpha u}, \tag{11}$$

$$S_{-1} = E(w) - E(\alpha), \quad S_0 = \frac{1}{\alpha}\left({\rm e}^{-w} - {\rm e}^{-\alpha}\right),$$

$$S_1 = \frac{1}{\alpha^2}\left[{\rm e}^{-w}(w+1) - {\rm e}^{-\alpha}(\alpha+1)\right],$$

$$S_2 = \frac{1}{\alpha^3}\left[{\rm e}^{-w}(w^2+2w+2) - {\rm e}^{-\alpha}(\alpha^2+2\alpha+2)\right], \tag{12}$$

where $w = \alpha u_1$, $E(x)$ is the integral exponent, which can be easily calculated using, for instance, Equation (21) of the article of Baiko and Yakovlev (1995).

The natural generalization of Equation (10) to the case of large–size nuclei can be provided by the following expressions:

$$K_0 = 2\Phi_1\left[1 + \frac{(18\pi Z)^{2/3} g^2 \Phi_2}{5\Phi_1 P_0}\right]^{-P_0}, \tag{13}$$

$$K_2 = \frac{1}{2}\Phi_0\left[1 + \frac{(18\pi Z)^{2/3} g^2 \Phi_1}{5\Phi_0 P_2}\right]^{-P_2}, \tag{14}$$

where P_0 and P_2 are the fit parameters. These expressions describe quite accurately our numerical results with $P_0 = 4.787 - 0.0346\,Z$ and $P_2 = 2.729 - 0.0204\,Z$. The mean fit error of Equation (13) is 2%; the maximum error 4.7% takes place at $\alpha = 0.04$, $Z = 60$ and $g = 0.3$. The mean fit error of (14) is 2.3%, and the maximum error 10% takes place at $\alpha = 12$, $Z = 60$ and $g = 0.4$.

If $g \ll 1$, Equations (13) and (14) reproduce the fit expressions (18) – (27) of the article of Baiko and Yakovlev (1995). The latter equations are valid at rather low densities 10^3 g/cm^3 $\lesssim \rho \lesssim 10^{11}$ g/cm^3, at which the finite sizes of the nuclei are unimportant. Thus Equations (13) and (14) cover very large density range 10^3 g/cm^3 $\lesssim \rho \lesssim 10^{14}$ g/cm^3 (outer and inner neutron star crusts) and are valid for any nuclear composition.

4 ELECTRIC AND THERMAL CONDUCTIVITIES

Let us analyze the electric and thermal conductivities of electrons in crystalline matter of a neutron star crust. The nuclear composition of matter is not definitely known. For illustration, consider two well established models: ground state matter and accreted matter.

Ground state matter corresponds to the minimum of free energy per one baryon. This matter can be produced from hot dense matter of a newly born neutron star in the course of the subsequent stellar cooling. At densities $\rho < \rho_{\rm d} \approx 4 \times 10^{11}$ g/cm^3 (below the neutron drip, Section 2) we will use the composition of the ground state matter calculated by Haensel and Pichon (1994) on the basis of new laboratory measurements of masses of nuclei with large neutron excess. At $\rho > \rho_{\rm d}$ we will use the results of Negele and Vautherin (1973) derived with the aid of a modified Hartree–Fock method.

The nuclear composition of accreted matter is determined (Haensel and Zdunik, 1990a, b) by nuclear transmutations (pycnonuclear reactions, β-captures, emission and absorption of neutrons, etc) in cold dense accreted matter sinking within the star. The results are practically insensitive to the accretion rate and initial chemical composition. The accreted matter is assumed to burn into ^{56}Fe at $\rho \lesssim 10^7$ g/cm^3.

Both models of matter are formally calculated at $T = 0$, but they are actually valid at $T \lesssim 4 \times 10^9$ K (as long as the thermal effects do not influence the properties of nuclei). It is adopted that single species of nuclei is present at every pressure (density). This leads to jumps of the nuclear composition (A, Z) with the growth of pressure (density) and to jumps of typical temperatures depicted in Figures 1 and 2. At $\rho \lesssim 10^7$ g/cm^3 matter consists of ^{56}Fe in both models. At higher densities, the compositions of ground state and accreted matters are noticeably different. The accreted matter consists of lighter nuclei with lower Z. For instance, at $\rho = 4 \times 10^{12}$ g/cm^3 the accreted matter contains neutron rich magnesium nuclei, $A = 44$, $Z = 12$, while the ground state matter contains tin nuclei, $A = 159$, $Z = 50$. The difference of compositions affects the thermodynamic and kinetic properties of matter. For example, at 10^{11} g/cm^3 $\lesssim \rho \lesssim 10^{13}$ g/cm^3 the melting temperature of the accreted matter is a factor of 3 — 10 lower, than that of the ground state matter.

One should know the proton core radius $r_{\rm c}$, for calculating the thermal and electric conductivities. Following Itoh et al. (1984) we set: $r_{\rm c} = 1.15\, A^{1/3}$ fm at $\rho < \rho_{\rm d}$; $r_{\rm c} = 1.83\, Z^{1/3}$ fm at $\rho > \rho_{\rm d}$. It is easy to verify that $g = r_{\rm c}/a \lesssim 0.2$ for both models. Figure 3 shows the functions F_σ and F_κ versus $T/T_{\rm p}$ for a body-centered-cubic lattice of nuclei $A = 159$, $Z = 50$ ($\rho = 4 \times 10^{12}$ g/cm^3). The curves are qualitatively the same as in matter of lower density ($\rho < 10^{11}$ g/cm^3; see Baiko and Yakovlev, 1995). The allowance for the nuclear size decreases $F_{\sigma,\kappa}$ and the effective electron collision frequencies $\nu_{\sigma,\kappa}$, i.e., increases the electric and thermal conductivities. However, the effect is not strong, about (20 — 30)%. This is clearly seen from the integrals (6): the nuclear formfactor reduces the integrands with the growth of g only at large dimensionless momentum transfers $u \approx 1$ (i.e., at large–angle scattering), at which the integrands themselves are sufficiently small. The latter smallness is due to the Debye–Waller factor (which suppresses collisions with

large momentum transfers) and due to the factor $(1-\beta^2 u)$, that describes reduction of backward scattering of relativistic electrons.

Figure 4 shows the dependence of $F_{\sigma,\kappa}$ on $T/T_{\rm p}$ for the same conditions as in Figure 3, but for the face-centered-cubic lattice. As in a lower–density matter (Baiko and Yakovlev, 1995), the lattice type affects strongly the kinetic coefficients. The finite sizes of the nuclei again influence the result weakly, as in the body-centered-cubic lattice.

Figures 5 and 6 display the density dependence of the electric and thermal conductivities for the ground state and accreted matters at $T = 10^8$ and 5×10^8 K. At low ρ the curves are broken in melting points (Figures 1 and 2). The discontinuities of the kinetic coefficients are associated with the jumps of nuclear compositions (see above). At 10^{12} g/cm^3 $\lesssim \rho \lesssim 10^{13}$ g/cm^3 the electric and thermal conductivities of the accreted matter are a factor of 2 — 3 higher, than those of the ground state matter. This is naturally explained by lower nucleus charge (and lower electron collision frequencies) in the accreted matter.

Note that earlier the thermal and electric conductivities of the ground state matter in the inner crust of a neutron star was calculated and fitted by Itoh et al. (1984). Our results agree mainly with the results of these authors. However, there is a 30 — 50 % difference in the thermal conductivity at densities $\rho \gtrsim 10^{13}$ g/cm^3. Let us emphasize that our fit expressions are much simpler than those of Itoh et al. (1984), and they are valid for matter with any nuclear composition.

5 THERMAL DRIFT OF THE MAGNETIC FIELD

If the magnetic field is present in the stellar plasma, various thermal magnetic effects may operate (Urpin and Yakovlev, 1980). For instance, the Hall component of the thermopower affects the thermal flux, that emerges from the star, and induces the thermal drift of the magnetic field. If the field is not too large, so that the electron gas is weakly magnetized ($\omega_{\rm B}\,\tau \ll 1$, where $\omega_{\rm B} = eB/(cm_*)$), one can neglect the back reaction of the field onto the thermal flux. According to Equations (5) and (7), at $T \gtrsim T_{\rm p}$ one has $F_\sigma \approx F_\kappa$. This allows us to introduce the electron relaxation time $\tau_0(\varepsilon) = \nu_\sigma^{-1} = \nu_\kappa^{-1}$, which is the same for the thermal and electric conductions (ε being the electron energy). Under formulated conditions, the drift velocity u is parallel to the thermal flux Q (Urpin and Yakovlev, 1980)

$$u = \frac{2\eta Q}{n_{\rm e} p_{\rm F} v_{\rm F}} \approx 72\eta \frac{\sqrt{1+x^2}}{x^5}\left(\frac{T_e}{10^6\ {\rm K}}\right)^4 \ \frac{\rm m}{\rm yr}, \tag{15}$$

$$\eta = \frac{1}{2}\ \frac{\partial \ln(\tau_0(\varepsilon)\varepsilon^{-1})}{\partial \ln p}\bigg|_{p=p_{\rm F}}. \tag{16}$$

Here, we have assumed that $Q = \sigma_0 T_e^4$, where T_e is the effective temperature of the stellar surface and σ_0 is the Stefan – Boltzmann constant. The factor $\eta \sim 1$ and can change sign,

that corresponds to different thermal drift directions. Taking the derivative, we have

$$\eta \;=\; 1.5-\beta^2-\frac{2G_0(t)}{F_\sigma}\left[(1-\beta^2)e^{-\alpha}\frac{|f(2p_{\rm F}/\hbar)|^2}{|\epsilon(2p_{\rm F}/\hbar)|^2}+\beta^4\int_{u_0}^1 {\rm d}u\,\frac{|f(q)|^2}{|\epsilon(q)|^2}\,u\,{\rm e}^{-\alpha u}\right]. \quad (17)$$

The dashed line in Figures 1 and 2 shows those densities and temperatures at which $\eta = 0$. One has $\eta > 0$ above this line, i.e., the thermal drift is directed outward, and $\eta < 0$ below the line, so that the magnetic field drifts inward.

Note that Equations (15) and (16) are actually valid only at $T_{\rm p} \lesssim T \lesssim T_{\rm m}$, and the dashed line is broken when T reaches $T_{\rm m}$ with the growth of ρ. It is seen that the thermal drift can be directed either inward or outward in the above temperature range and at densities up to 10^{10} – 10^{11} g/cm^3. At higher densities and $T \gtrsim T_{\rm p}$, the factor η remains positive for the ground state matter. As for the accreted matter, $T_{\rm m}$ exceeds $T_{\rm p}$ at these densities, and Equation (16) becomes invalid. Calculation of the thermal drift at $T \lesssim T_{\rm p}$ is outside the scope of the present article.

6 CONCLUSIONS

We have calculated the thermal and electric conductivities of relativistic degenerate electrons due to electron–phonon scattering in Coulomb crystals of atomic nuclei at densities 10^{11} g/cm$^3 \lesssim \rho \lesssim 10^{14}$ g/cm^3, corresponding to the inner crust of a neutron star. Calculations are done with the aid of the approximate analytic method (Baiko and Yakovlev, 1995) taking exact spectrum of phonons and the Debye–Waller factor into account. In addition, we have taken into consideration finite sizes of atomic nuclei.

The results are fitted by a few simple equations which reproduce also the fit expressions obtained by Baiko and Yakovlev (1995) for lower densities. Thus we have obtained the unified fits which describe the thermal and electric conductivities in the wide density range 10^3 g/cm$^3 \lesssim \rho \lesssim 10^{14}$ g/cm^3 (in the inner and outer crusts of neutron stars) below the melting temperature but above the temperature where the Umklapp processes are frozen out, for the body-centered-cubic and face-centered-cubic crystals. Note that the same equations are valid in the presence of a weak magnetic field ($\omega_{\rm B}\,\tau \ll 1$).

Our results can be useful for numerical simulations of thermal evolution of neutron stars (cooling, nuclear burning of accreted matter) and evolution of their magnetic fields (ohmic dissipation, generation due to thermal magnetic effects).

ACKNOWLEDGEMENTS

This work was partly supported by the Russian Foundation for Basic Researches (grant No. 93-02-2916), the International Science Foundation (grant No. R6-A000), and INTAS (grant No. 94-3834). One of the authors (D.A. Baiko) is also grateful to the International Science Foundation the for undergraduate grant No. 555s.

REFERENCES

Baiko, D.A. and Yakovlev, D.G., Astron. Lett., 1995, vol. 21, p. 702.
Carr, W.J., Phys. Rev., 1961, vol. 122, p. 1437.
Haensel, P. and Zdunik, J.L., Astron. Astrophys., 1990a, vol. 227, p. 431.
Haensel, P. and Zdunik, J.L., Astron. Astrophys., 1990b, vol. 229, p. 117.
Haensel, P. and Pichon, D., Astron. Astrophys., 1994, vol. 283, p. 313.
Itoh, N., Kohyama, Y., Matsumoto, N., and Seki M., Astrophys. J., 1984, vol. 285, p. 758; erratum vol. 404, p. 418.
Itoh, N., Hayashi, H., Kohyama, Y., Astrophys. J., 1993, vol. 418, p. 405.
Jancovici, B., Nuovo Cimento, 1962, vol. 25, p. 428.
Lorenz, C.P., Ravenhall, D.G., and Pethick C.J., Phys. Rev. Lett., 1993, vol. 70, p. 379.
Nagara, H., Nagata, Y., and Nakamura, T., Phys. Rev., 1987, vol. A36, p. 1859.
Negele, J.W. and Vautherin, D., Nucl. Phys., 1973, vol. A207, p. 298.
Raikh M.E. and Yakovlev D.G., Astrophys. Space Sci., 1982, vol. 87, p. 193.
Shapiro, S.L. and Teukolsky, S.A., Black Holes, White Dwarfs, and Neutron Stars, New York: Wiley-Interscience, 1993.
Urpin, V.A. and Yakovlev, D.G., Sov. Astron., 1980, vol. 24, p. 325.
Yakovlev, D.G. and Urpin, V.A., Sov. Astron., 1980, vol. 24, p. 303.

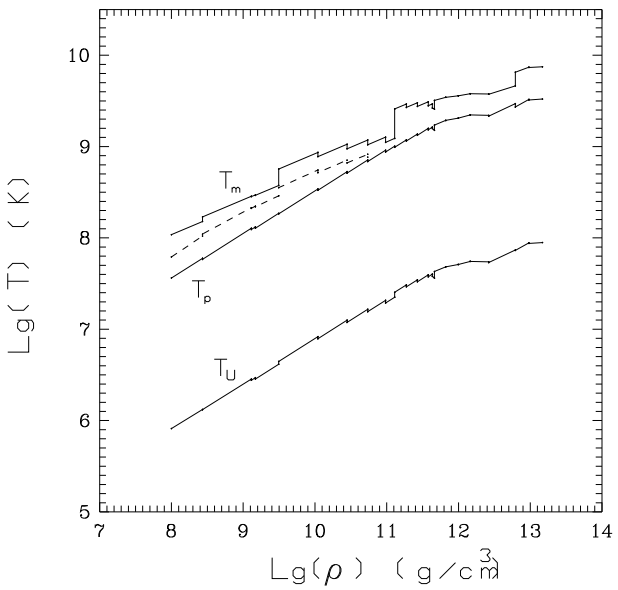

Figure 1: Density — temperature diagram for the ground state matter: $T_{\rm m}$ is the melting temperature, $T_{\rm p}$ is the ion plasma temperature, $T_{\rm U}$ is the freezing temperature of Umklapp processes. Dashed line corresponds to the conditions at which the thermal drift velocity equals zero.

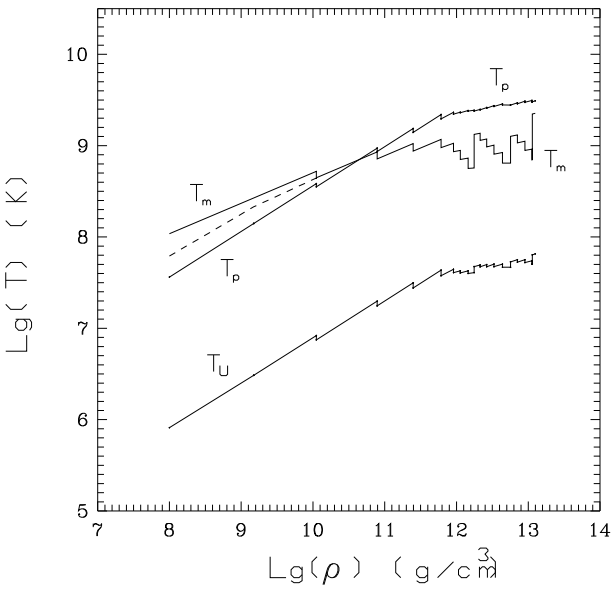

Figure 2: Same as in Figure 1 but for the accreted matter.

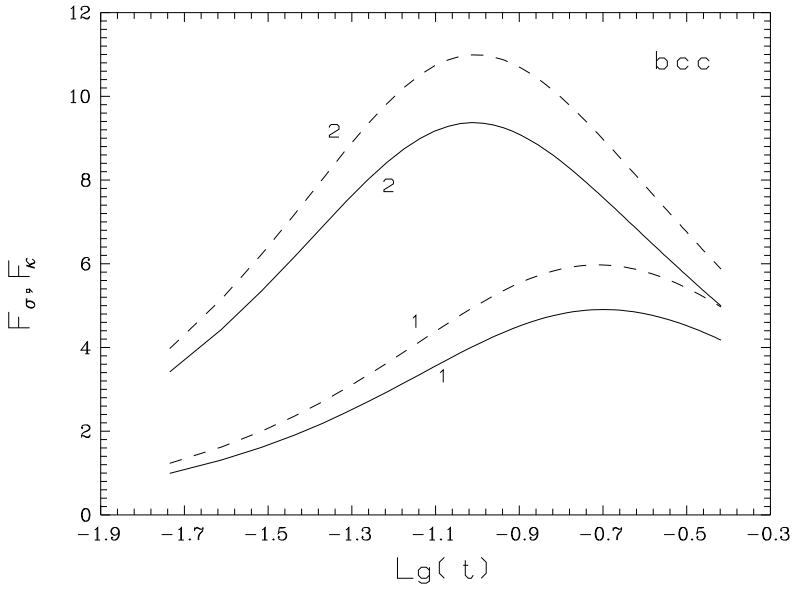

Figure 3: Factors F_σ (curves 1) and F_κ (curves 2) versus $t = T/T_{\rm p}$ for the body-centered-cubic and face-centered-cubic crystals composed of ^{159}Sn nuclei at density $\rho = 4 \times 10^{12}$ g/cm^3 with account for the finite nucleus size ($g = 0.15$, solid lines) and for the point–like nuclei ($g = 0$, dashes).

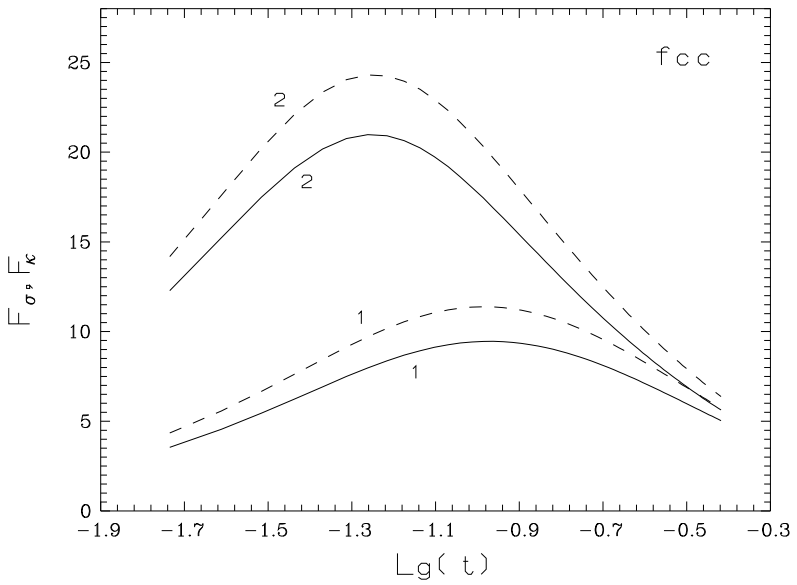

Figure 4: Same as in Figure 3 but for the face-centered-cubic crystal.

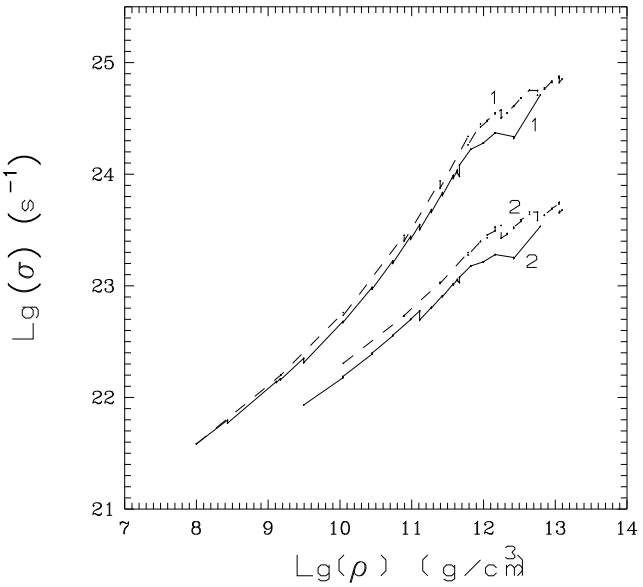

Figure 5: Electric conductivity versus density for the ground state (solid lines) and accreted (dashes) matters at $T = 10^8$ K (curves 1) and $T = 5 \times 10^8$ K (curves 2).

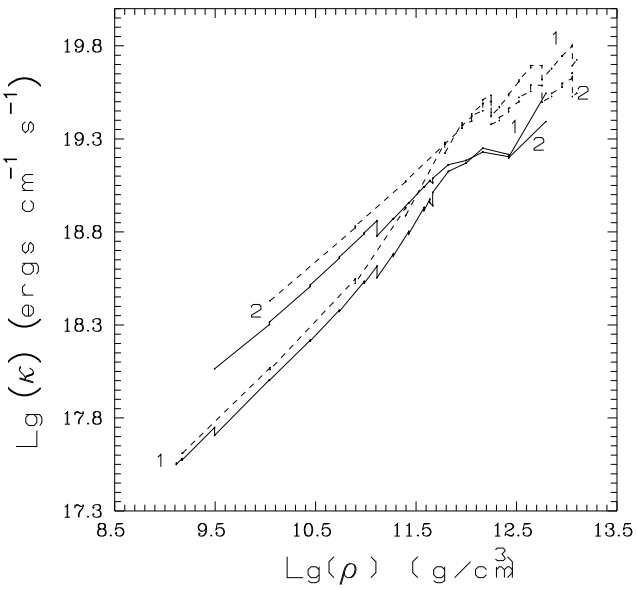

Figure 6: Thermal conductivity versus density for the same conditions as in Figure 5.